JGR Atmospheres

RESEARCH ARTICLE
10.1029/2020JD032745

A Statistical Analysis of the Energy Dissipation Rate Estimated From the PMWE Spectral Width in the Antarctic

M. Kohma[1], K. Sato[1], K. Nishimura[2], M. Tsutsumi[2], and T. Sato[3]

[1]Department of Earth and Planetary Science, Graduate School of Science, University of Tokyo, Tokyo, Japan, [2]National Institute of Polar Research and The Graduate University for Advanced Studies (SOKENDAI), Tokyo, Japan, [3]Institute for Liberal Arts and Sciences, Kyoto University, Kyoto, Japan

Key Points:
- The turbulent kinetic energy dissipation rates in the Antarctic mesosphere from PMWE spectral widths are estimated
- The dissipation rates at heights of 55–82 km are in the range of 10^{-4} to 10^{0} m^2 s^{-3}
- The summer-to-winter (winter-to-summer) transition of the turbulence parameters occurs in April (September)

Supporting Information:
- Supporting Information S1

Correspondence to:
M. Kohma,
kohmasa@eps.s.u-tokyo.ac.jp

Citation:
Kohma, M., Sato, K., Nishimura, K., Tsutsumi, M., & Sato, T. (2020). A statistical analysis of the energy dissipation rate estimated from the PMWE spectral width in the Antarctic. *Journal of Geophysical Research: Atmospheres*, *125*, e2020JD032745. https://doi.org/10.1029/2020JD032745

Received 20 MAR 2020
Accepted 16 JUL 2020
Accepted article online 31 JUL 2020

Abstract The radar volume reflectivity and turbulent kinetic energy dissipation rate in the Antarctic mesosphere were estimated from the polar mesosphere winter echoes (PMWE) recorded using a vertical beam of the PANSY radar, a Mesosphere-Stratosphere-Troposphere radar at Syowa Station (69°S, 40°E), over a period of 4 years. The observed radar volume reflectivity exhibits a lognormal distribution in the range of 2×10^{-18} to 5×10^{-15} m^{-1} for a height region of 55–82 km. The turbulent energy dissipation rate estimated from the spectral widths of the PMWE ranges from 10^{-4} to 10^{0} m^2 s^{-3}. From monthly histograms of the turbulent energy dissipation rate for a fixed solar zenith angle (SZA) and height, it was found that the summer-to-winter transition of the turbulent energy dissipation rate occurs in March, while the winter-to-summer transition occurs in September. This seasonal variation agrees well with that of gravity wave activity, suggesting that the turbulence in the mesosphere is likely caused by gravity wave breaking.

1. Introduction

Polar mesosphere winter echoes (PMWEs) are VHF radar echoes observed in the 55–80 km height region in both hemispheres (Czechowsky et al., 1989; Ecklund & Balsley, 1981; Morris et al., 2011). The mechanism of PMWE is not fully understood since these echoes are less frequent and weaker than the polar mesosphere summer echoes (PMSEs) that are observed mainly in the 80–92 km height region. Several mechanisms for PMWE that have been previously suggested include strong air turbulence (Lübken, 2014; Lübken et al., 2006, 2007; Tsutsumi et al., 2017) and highly damped ion-acoustic waves (Kirkwood, 2007; Kirkwood, Belova, et al., 2006) in the ionized atmosphere. Recent studies have suggested that the large Schmidt number associated with charged meteor smoke particles may be responsible for the appearance of PMWE (e.g., Kavanagh et al., 2006; La Hoz & Havnes, 2008).

Observational studies have indicated that large electron density is critical to the existence of PMWE. PMWEs are frequently observed during sunlit conditions in the height region of 55–82 km, while, during the nighttime, the frequency of PMWE decreases, and the lower edge height of PMWE increases (Latteck & Strelnikova, 2015; Nishiyama et al., 2015). The local time dependence of the height distribution of PMWE is well reproduced by the theoretical calculation of the radar volume reflectivity associated with turbulence in the ionized atmosphere (Latteck & Strelnikova, 2015). Previous studies have reported PMWE occurrence in association with ionospheric disturbances, including geomagnetic disturbances, solar proton events, and auroral breakups (e.g., Kataoka et al., 2019; Nishiyama et al., 2018; Tsutsumi et al., 2017).

The spectral widths of PMWE have been investigated in several earlier studies. Kirkwood, Belova, et al. (2006) investigated 1-day observations of PMWE by the EISCAT 224-MHz radar (69.6°N, 19.2°E) and showed that there is no significant difference in the spectral widths between inside the PMWE and echoes from the background plasma around the PMWE. Strelnikova and Rapp (2013) reexamined the PMWE spectral widths using a large number of PMWE observations and showed substantial variability. According to Lübken et al. (2007) and Strelnikova and Rapp (2013), the frequency spectra of backscatter signals inside PMWE layers tend to have a Gaussian shape, which indicates that the scattering echoes are related to neutral air turbulence. If the main source of PMWE appearance is explained by the turbulence in the ionized atmosphere, the spectral widths of PMWE are related to the turbulent kinetic energy dissipation rate ε (Hocking, 1999).

Strelnikova and Rapp (2013) showed an increase in the spectral widths with height in the Arctic mesosphere during winter. The present study also estimates the turbulence parameters in the Antarctic based on the assumption that PMWEs are scattering echoes associated with turbulence in the ionized atmosphere.

The turbulence parameters in the mesosphere have been estimated by in situ rocket observations. Lübken (1997) showed a clear seasonal contrast of ε in the high-latitude mesosphere: In summer, a maximum ε of 0.15 $m^2\ s^{-3}$ is observed around a height of 90 km, and significant turbulent layers are confined to 78–97 km height region. In winter, the values of ε are relatively small (10^{-3} to $2 \times 10^{-2}\ m^2\ s^{-3}$) compared to those in summer, and the turbulent layers are detected in the height range of 60–80 km. Since frequent rocket observations are costly, a detailed assessment of the seasonal variation of the mesospheric ε has not been available. Estimation of the turbulence parameters in the mesosphere based on MF radar observations has also been performed. However, MF radars inherently assign overestimated values to these turbulence parameters (e.g., Hall et al., 1999; Holdsworth et al., 2001). Hall et al. (1999) showed that the mesospheric turbulence intensity in the Arctic in the height range of 60–80 km is maximized during winter. It should be noted that the seasonal variation of mesospheric turbulence parameters based on in situ or radar observations over Antarctica has, to our knowledge, not yet been investigated.

The present study examines the seasonal variation of mesospheric radar volume reflectivity and turbulence parameters estimated from PMWE observations recorded over a 4-year period by the Program of the Antarctic Syowa Mesosphere-Stratosphere-Troposphere/Incoherent Scatter (PANSY) radar, a VHF clear-air Doppler radar installed at Syowa Station (69.00°S, 39.35°E) (Sato et al., 2014). Recently, Kohma et al. (2019) examined the seasonal and height variation of ε in the troposphere and lower stratosphere using the PANSY radar observations. While continuous observation in the troposphere and lower stratosphere is possible, PMWE spectral widths in the mesosphere are derived mainly in the daytime, when the PMWE can be more frequently observed. It should be noted that the histograms of the spectral widths and ε estimated for the mesosphere are weighted by the PMWE occurrence probability distribution. Thus, we discuss the seasonality of the mesospheric ε by taking sampling bias into consideration.

The remainder of the paper is organized as follows: A description of the data and the method for estimating ε from the PMWE spectral widths are presented in section 2; the seasonal variation and height dependence of the volume reflectivity of PMWE and ε are described in section 3; and a summary and concluding remarks are given in section 4.

2. Data and Methodology

The PANSY radar is the first Mesosphere-Stratosphere-Troposphere/Incoherent Scatter (MST/IS) radar in the Antarctic region (Sato et al., 2014). Continuous observations have been made by a partial system of the PANSY radar since 30 April 2012. The radar has been in almost continuous full-system operation since late September 2015. We used observation data from the full system of the radar for March through October over the 4-year period from 2016 to 2019. The interpulse period (IPP) was 800 μs, except for the periods of 1 March to 8 April and 26 June to 10 July 2019, when the IPP was set to 1,600 μs. The time resolution of the observation was ~70 (150) s for the IPP of 800 (1,600) μs, while the observation time intervals were ~200 (310) s because of interleaving observations for the troposphere and stratosphere. The record length is 128, and the number of incoherent integration is 10. The range resolution was 600 m along the beam direction. We used vertical beam measurements in order to avoid possible spectral broadening caused by the vertical shear of horizontal winds (shear broadening). Note that the effect of partial reflection is considered negligible in the mesosphere (Fukao et al., 2014; Hocking et al., 2016). The analyses were made for the height range of 55 to 82 km, where most PMWEs are observed (e.g., Tsutsumi et al., 2017). The number of vertical profiles of PMWE was ~12,000 per month on average during the analyzed period. The radar parameters are shown in Table 1. Details of the PANSY radar are given in Sato et al. (2014).

Radar volume reflectivity η is defined as backscatter cross section per unit volume. The calculation for radar volume reflectivity was performed following Sato et al. (2014, 2017). The minimum η with a detectability threshold of 3 taken for the present radar observations was approximately $1 \times 10^{-18}\ m^{-1}$. Note that since previous studies of PMWE using the PANSY radar (Nishiyama et al., 2015, 2018; Tsutsumi et al., 2017) are based on observations using the above-mentioned partial system, the minimum detectable η for these studies is approximately 10 times larger than that of the present study. We assumed that the scattering volume is

Table 1
Parameters of the PANSY Radar

Title	Value
Location	Syowa Station, Antarctic (69.00°S, 39.35°E)
Effective antenna area	About 18,000 m^2
Operating central frequency	47.0 MHz
Peak power output	520 kW
Interpulse period	1,600 μs (1 March to 8 April 8 and 26 June 10 July 2019), 800 μs (otherwise)
Pulse code	16-element Spano code (1 March to 8 April 8 and 26 June to 10 July 2019), eight-element Spano code (otherwise)
Duty factor	4%
FFT number	128
Number of coherent integrations	16 times
Number of incoherent integrations	10 times
Range resolution	600 m
Number of beams	5 (vertical + 10° oblique to NSE and W.)

filled by turbulence although the sparsity of PMWE might cause underestimation of η of the PMWE (Kirkwood, Chilson, et al., 2006).

The turbulence parameters were derived from the spectral widths of PMWE following Sato and Woodman (1982) and Hocking (1983). The calculation for the turbulent velocity variance followed the approach of Kohma et al. (2019) and Nishimura et al. (2020). Since the two-way beam pattern was not axially symmetric due to the irregular antenna distribution of the PANSY radar (Sato et al., 2014), we extracted the turbulent velocity variance considering the antenna distribution. Nishimura et al. (2020) derived a theoretical relation between the turbulence spectrum and observed echo spectrum and proposed a debroadening algorithm taking the two-way beam pattern and wind vector into consideration. The beam broadening component can be subtracted with a deconvolution operation for the measured echo spectra. According to this theoretical calculation by Nishimura et al. (2020), the conventional method (e.g., Fukao et al., 2014) overestimates the beam broadening, which causes significant underestimation (sometimes even giving negative values) of the turbulent velocity variance (e.g., Dehghan & Hocking, 2011; Nastrom, 1997). In our study, the spectral widths due to turbulence were estimated using a Gaussian fitting from the spectra after the beam broadening component was subtracted. This study did not consider the time broadening effect, which is normally small compared to beam broadening (Nastrom & Eaton, 1997; Sato et al., 1995). The square of the turbulent spectral widths (σ^2_{turb}) used in the following analyses did not include negative values. The turbulent velocity variance $\overline{v'^2}$ is proportional to σ^2_{turb} through the relation $\overline{v'^2}=\sigma^2_{\mathrm{turb}}(\lambda/2)^2/(2\ln 2)$, where λ is the radar radio wavelength (6.4 m for the PANSY radar).

The velocity variance due to turbulence in a stably stratified flow is related to the energy dissipation rate as follows (Hocking, 1983; Weinstock, 1981):

$$\varepsilon \approx c_{\mathrm{R}}\overline{v'^2}N,$$

where N is the buoyancy frequency. According to Hocking et al. (2016), an appropriate value range for the proportional constant c_{R} is 0.5 ± 0.25. In the present study, N and c_{R} were set to 0.02 s^{-1} and 0.45, respectively, as typical values.

3. Results

3.1. Radar Volume Reflectivity

Figure 1 shows the time-height sections of daily average volume reflectivity η in March through October of 2016–2019. As noted in section 2, observation has been nearly continuous (purple lines at the bottom for each panel). Most PMWEs are observed in the 55–82 km height range, most frequently at a height of approximately 70 km. The height range of the PMWE tends to be broad in April, May, August, and September compared to that in March, June, and October. The midwinter minimum of the PMWE height range is likely related to the duration of sunlit time (Nishiyama et al., 2015). It is interesting that monthly and

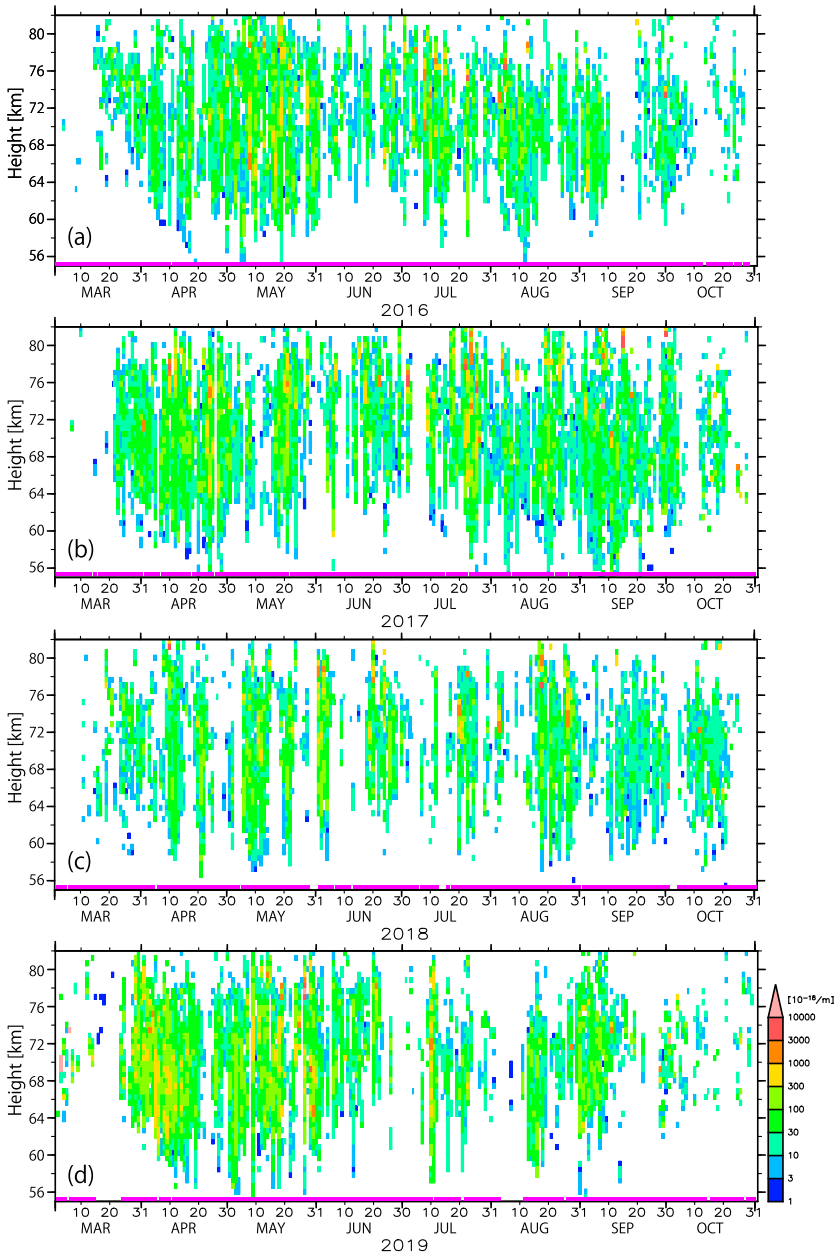

Figure 1. Time-height sections of daily average volume reflectivity of PMWE observed by the vertical beam for (a) 2016, (b) 2017, (c) 2018, and (d) 2019. Only the areas where PMWE is detected more than 10 times are colored. The time periods of the observations are denoted by purple horizontal lines at the bottom of each panel.

submonthly time scale variations in the appearance of PMWE are also observed. Although interannual variability of PMWE appearance is out of the scope of the present study, it is noteworthy that the frequency of PMWE in 2017 is higher than in other years. In the discussion that follows, the focus is on statistics averaged over the 4 years of the study.

Figure 2 shows the normalized histogram of $\log_{10}(\eta)$ created from all PMWE observations over the 4-year period for the height range of 55–82 km. As shown, the range of η is 2×10^{-18}–5×10^{-15} m^{-1}, and its median value is 3×10^{-17} m^{-1}. The distribution is approximately lognormal, with a cutoff in the left tail. The minimum volume reflectivity detectable by the PANSY radar is an order of 10^{-18} m^{-1}, which roughly corresponds to the cutoff in the left tail of the distribution.

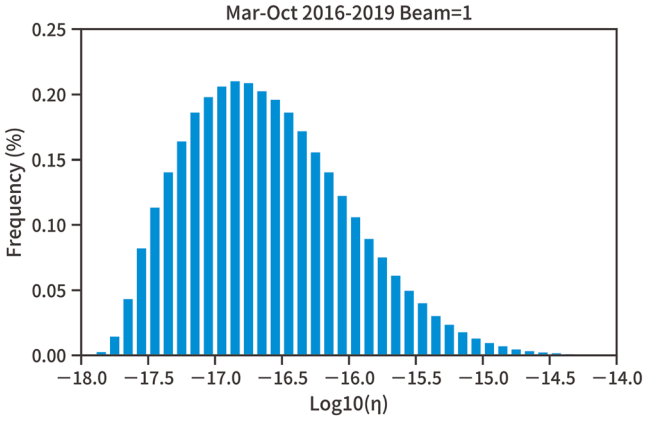

Figure 2. A histogram of the logarithm of volume reflectivity in m^{-1} based on PMWE observations over 4 years and over the height range of 55–82 km.

Latteck et al. (2019) showed the distribution of PMWE volume reflectivity based on 8-year observations by the MAARSY radar at Andøya (69.30°N, 16.04°E). The value range of the volume reflectivity in the present study is quite similar to their result, although the median value is slightly smaller in the present study. While a comparison of η between the Arctic and Antarctic would be of significant interest, it should be noted that, for the comparison, we need to carefully consider the left tail of the distributions, which greatly depends on the sensitivity of the radar system being used.

Figure 3 shows the height dependence of the histograms of η for each month. The histograms are normalized by the number of vertical profiles. As noted, the height ranges of PMWE are wider in April, May, August, and September than in March, June, and October. The η median is maximized in the 65–70 km range in March through September.

We also found that the frequency of η values greater than 10^{-16} m^{-1} in the height range of 60–78 km is relatively high compared to the frequencies at heights above 78 km and below 60 km. According to PMWE theory based on the neutral air turbulence in the ionized atmosphere, volume reflectivity decreases with increases in kinematic viscosity ν (Hocking, 1985; Lübken, 2014). Thus, the low frequency of large η values at heights above 78 km is likely due to the exponential increase in ν with height. The low frequency of large η values below 60 km is explained by the small electron density (N_e). According to the theory of scattering echoes from turbulence, η increases with N_e except when N_e is extremely high, which can occur with strong ionospheric disturbances (Nishiyama et al., 2018; Rapp et al., 2002).

3.2. Energy Dissipation Rates From PMWE Spectral Widths

Figure 4 shows a normalized histogram of $\log_{10}(\varepsilon)$ in the height range of 55–82 km over the entire analyzed period. As shown here, the range of ε estimated by the PANSY radar is approximately 10^{-4} to 10^{0} m^2 s^{-3}. The histogram of ε has a peak around 5×10^{-2} m^2 s^{-3}, while the median value is ~2×10^{-3} m^2 s^{-3}, which indicates that the distribution is negatively skewed. The skewed distribution of ε is also seen in a two-dimensional histogram of η and ε (Figure S1 in the supporting information). Since ε was estimated using the spectral widths of the PMWE, the ε distribution and ε statistics are weighted by the PMWE probability distribution. In other words, the turbulence parameter results presented here are based on a conditional probability distribution given that PMWE are detected.

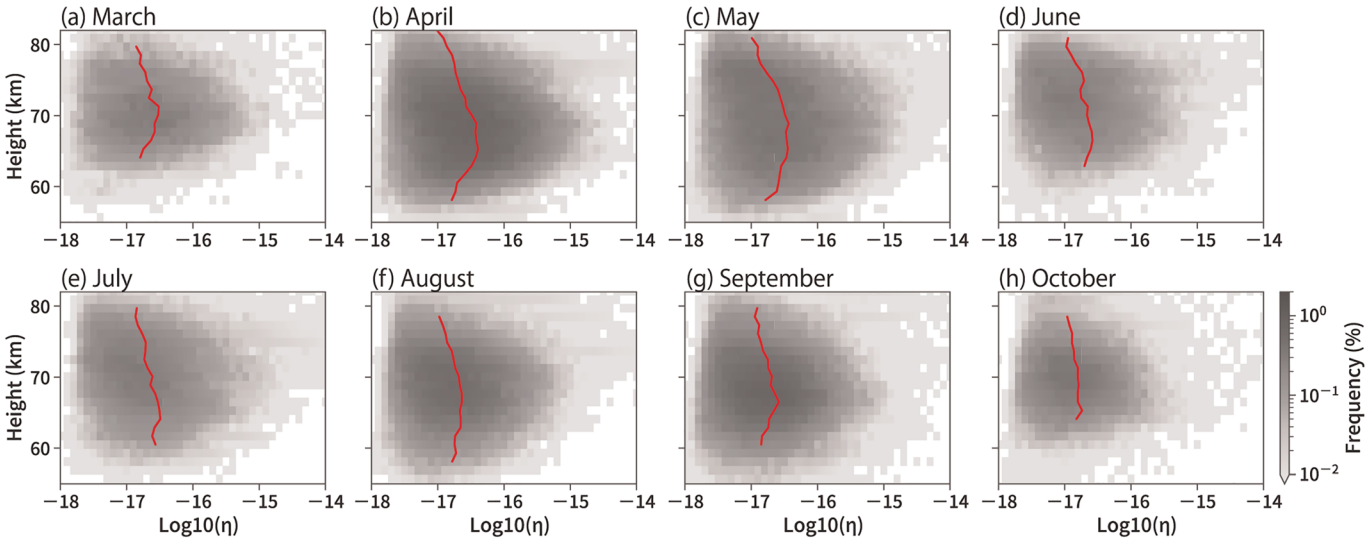

Figure 3. Distributions of η as a function of height for each month: (a) March, (b) April, (c) May, (d) June, (e) July, (f) August, (g) September, and (h) October. The red curves indicate the median values for each height.

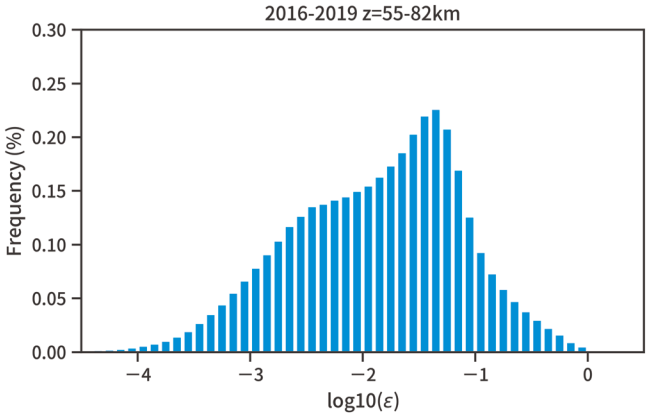

Figure 4. Same as Figure 2 but for the logarithm of ε in $m^2\ s^{-3}$.

In order to examine the effect of PMWE appearance on the histograms of ε, the height and solar zenith angle (SZA) dependence of ε are shown in Figures 5–7. First, normalized histograms of $\log_{10}(\varepsilon)$ in four height ranges of 60–65, 65–70, 70–75, and 75–82 km are shown in Figure 5. In 60–75 km, the histograms have negative skewness, similar to that in the whole analyzed height range (Figure 4). The distribution in 75–82 km is approximately lognormal and has a peak around $5 \times 10^{-2}\ m^2\ s^{-3}$. The lower frequency of these small ε values at greater heights is likely explained by the higher kinematic viscosity associated with height. According to the theory of scattering echoes from turbulence in the ionized atmosphere, sufficiently strong turbulence is required for PMWE to be detected by radar when kinematic viscosity is high.

Next, Figure 6 shows the value of ε estimated from the PMWE spectral widths as a function of height for each month. Above 78 km, the distributions in all analyzed months are approximately lognormal with a peak around $5 \times 10^{-2}\ m^2\ s^{-2}$. The frequencies of small ε (e.g., ε less than $10^{-2}\ m^2\ s^{-3}$, which is denoted by blue broken lines) above 78 km are significantly smaller compared to those in the height range of 60–78 km. In the height range of 60–74 km, the distributions of ε have a broad peak. Most ε's are on the order of 10^{-4} to $10^{-1}\ m^2\ s^{-3}$. Note that this range includes ε estimated from rocket observations in the Arctic winter (blue curves in Figure 6; Lübken, 1997). It is also noticeable that the frequency of ε values smaller than $10^{-3}\ m^2\ s^{-3}$ is low in June and July compared with that in other months. This is likely because the SZA is larger in June and July on average, and the mean N_e decreases with SZA.

The SZA dependence of the histogram of ε in the height range of 70–75 km is shown in Figure 7. The ε values are binned in 5° intervals. Because of the seasonal variation in the solar declination, observations for SZAs from 65° to 100° are available in March, while observations for SZAs greater than 90° are available in June.

From a comparison of PMWE frequencies between large and small SZAs, it can be seen that the PMWE frequency for SZAs less than 95° is significantly larger than for SZAs greater than 95° for all months. This indicates that the large N_e during sunlit time is a preferable condition of the presence of PMWE. Furthermore, it is found that, for SZAs greater than 95°, the frequencies of ε values less than $3 \times 10^{-3}\ m^2\ s^{-3}$ are quite small

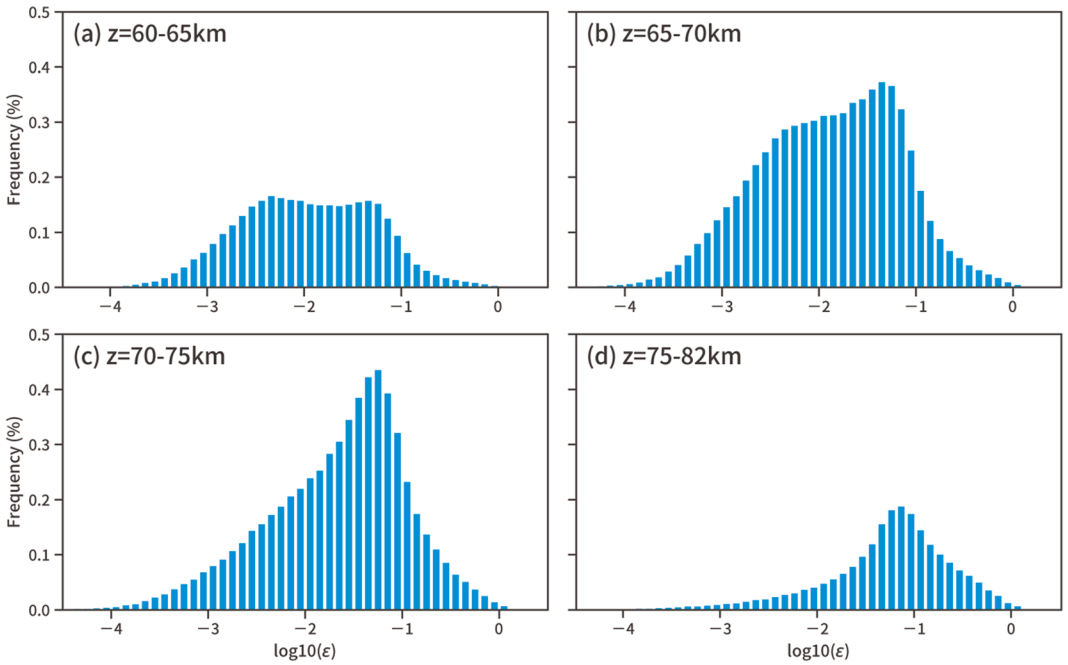

Figure 5. Same as Figure 4 but for the height ranges of (a) 60–65, (b) 65–70, (c) 70–75, and (d) 75–82 km.

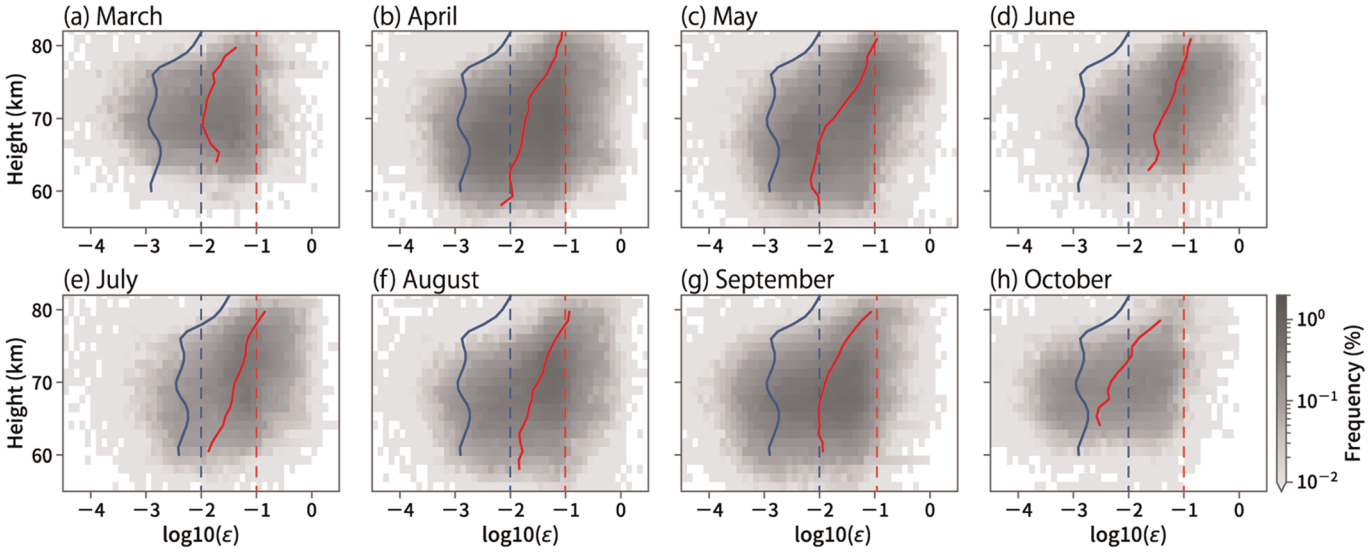

Figure 6. Distributions of the logarithm of ε as a function of height for each month: (a) March, (b) April, (c) May, (d) June, (e) July, (f) August, (g) September, and (h) October. Red thick curves indicate the median values for each height. Blue thick curves indicate the vertical profile of ε from Lübken (1997), who estimated ε from rocket observations in the Arctic winter. Blue (red) vertical broken lines indicate ε of 10^{-2} m^2 s^{-3} (10^{-1} m^2 s^{-3}).

compared to those greater than 3×10^{-3} m^2 s^{-3}. In addition, the ε median for SZAs greater than 95° is larger than that for SZAs less than 95° by a factor of 2 to 5. Since N_e is low during the nighttime compared to the daytime, sufficiently strong turbulence is required for PMWE to be detected by the radar. Thus, the distribution of ε from the PMWE spectral widths during the nighttime should be positively biased compared with those during the daytime.

Figure 8 shows the local time dependence of the monthly mean of ε and SZA in the height range of 70–75 km for each month. It is seen that PMWE appears when the SZA is 95 or less. PMWE tends to appear slightly

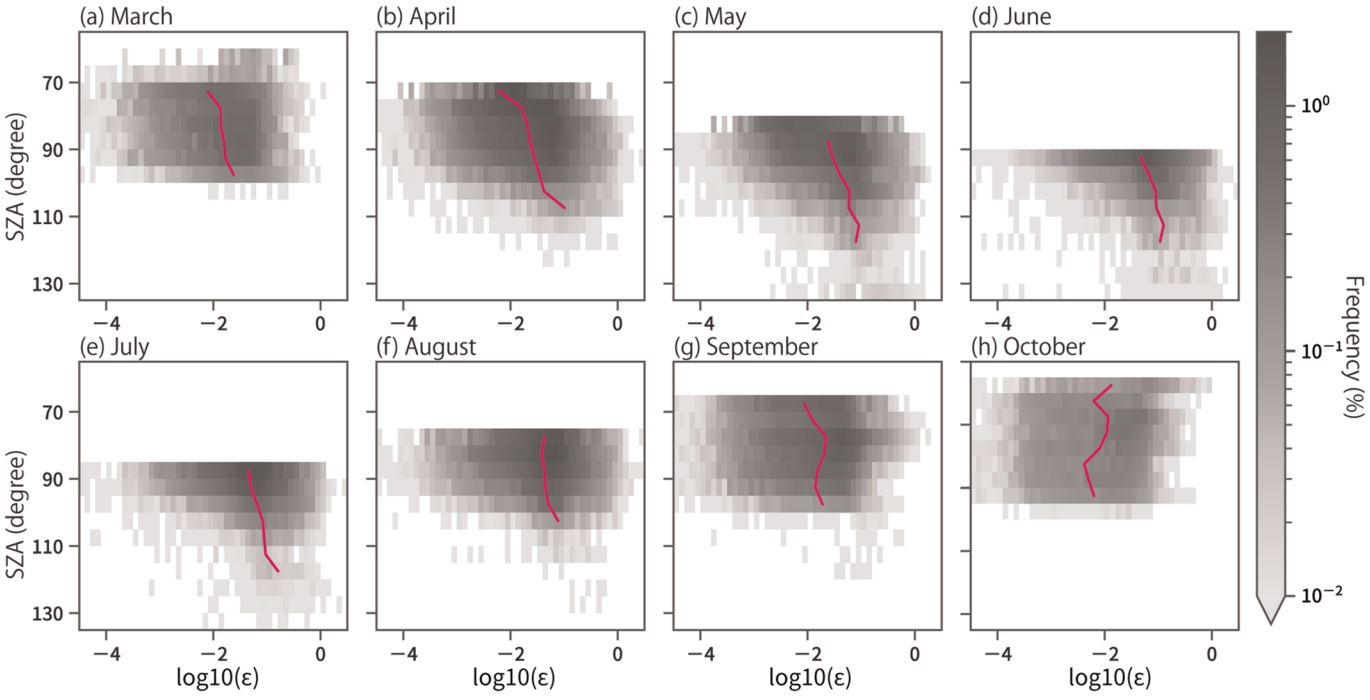

Figure 7. Distributions of the logarithm of ε in the height range of 70–75 km as a function of SZA for each month: (a) March, (b) April, (c) May, (d) June, (e) July, (f) August, (g) September, and (h) October. The red curves indicate the median values for each SZA.

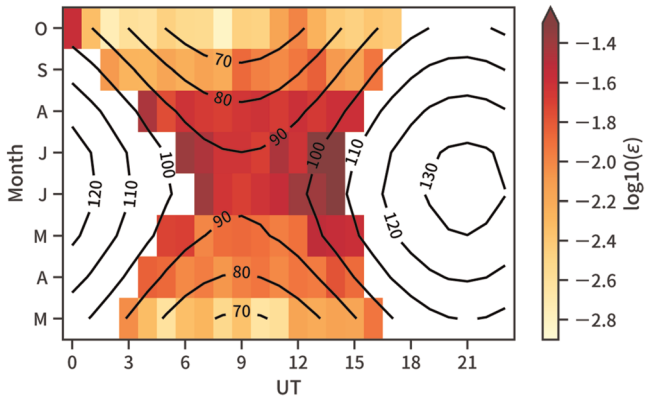

Figure 8. The local time dependence of the monthly mean of ε (color) and SZA (contour) in the height range of 70–75 km for each month. Only the areas where 10 or more values of ε are obtained are colored. The contour interval is 10°.

more frequently on the sunset than on the sunrise. These characteristics have also been noted in Nishiyama et al. (2015). In terms of monthly mean ε, from March to August, the ε tends to be higher at dawn and dusk than during the day. In addition, from the seasonal variation of ε at a specific local time, the maximum of the ε is observed from June to August. It is important to note, however, that the monthly mean ε's shown here are weighted by the PMWE probability distribution and therefore do not necessarily represent the actual local time or seasonal variation.

We conducted similar analyses for other height ranges. The results for the ranges of 65–70 and 75–82 km were qualitatively similar to those for 70–75 km. Below 65 km, the number of PMWE appearances for SZAs greater than 95° was so small that a comparison of the ε distributions between the daytime and nighttime could not be performed.

The relation between the estimated ε and PMWE can be summarized as follows: The height dependence of ν and N_e and the SZA dependence of N_e strongly affect the appearance of PMWE. Following the theory that PMWEs are attributable to the scattering echoes from turbulence in the ionized atmosphere, strong turbulence intensity is required for PMWE to be detected, particularly in greater height ranges or during the nighttime. As a result, the histogram of ε from the PMWE spectral widths averaged over the analyzed period and height range is negatively skewed (Figure 4).

3.3. Seasonal Variation of ε

In section 3.2, it is shown that the negatively skewed histogram of ε estimated from the PMWE spectral widths is likely due to the sampling bias associated with PMWE appearance. This means that the seasonal variation in the estimated ε value will also be affected by this bias. For example, small ε values would be undersampled in June because of the relatively short sunlit time compared to March and October. Thus, the median ε value shown for June would be larger than that for March and October, even if the ε values were constant during PMWE season. In order to produce a more reliable seasonal variation estimate of ε on a monthly time scale, the dependence of the radar volume reflectivity of the PMWE on the background parameters, including N_e and ν, should be considered. Lübken (2014) summarized the radar volume reflectivity of the scattering echoes from turbulence and showed that the radar volume reflectivity depends on several background parameters:

$$\eta = \eta(\varepsilon, \eta_{\mathrm{KOL}}, \mathrm{Sc}, \chi_n)$$
$$\chi_n = \chi_n(\varepsilon, N_e, dN_e/dz, \mathrm{Ri}, \mathrm{Pr}, N, H_N),$$

where η_{KOL} is the Kolmogorov microscale $(\nu^3/\varepsilon)^{1/4}$ and Sc, Ri, Pr, N, and H_N are the Schmidt number, Richardson number, Prandtl number, buoyancy frequency, and density scale height, respectively. The Schmidt number is defined as the ratio of ν to electron diffusivity. In order to discuss the seasonal variation of ε, the following analyses are conducted based on two assumptions: On a monthly time scale, (i) ν, Sc, Ri, Pr, N, and H_N at a certain height are constant during PMWE season, and (ii) N_e and dN_e/dz at a certain height depend only on the SZA and random solar/geomagnetic activities. The assumption that ν, Pr, and H_N are independent of season is likely valid. Although the mean N varies slightly on the monthly time scale during PMWE season, the monthly mean variation is, at most, 20% around a height of 70 km according to NRLMSISE-00 (Picone et al., 2002). The dependence of η on Ri comes from the expression of the eddy diffusion coefficient $K_m = \mathrm{Ri} \cdot \varepsilon/N^2$ in a stably stratified flow (Hocking, 1985). However, recent observational studies of the turbulent diffusion in the lower atmosphere and upper ocean suggest that the proportional coefficient between K_m and ε/N^2, which is known as the mixing coefficient, is constant (~0.2) in a statistical sense (e.g., Gregg et al., 2018; Kantha & Luce, 2018). Thus, the η dependence on Ri is likely small.

Several previous studies (e.g., Kavanagh et al., 2006; La Hoz & Havnes, 2008) have pointed out that the increase in Sc in the presence of charged aerosols could play a crucial role in the appearance of PMWE. However, the value of Sc in the winter mesosphere is still unclear. Due to the lack of knowledge

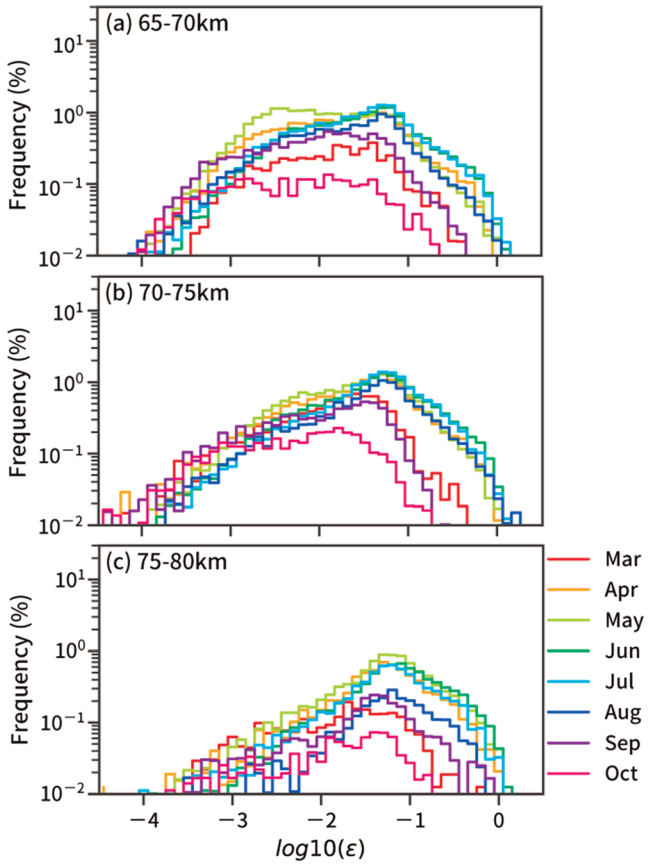

Figure 9. Histograms of the logarithm of ε for SZA from 90° to 95° in the height range of (a) 65–70 km, (b) 70–75 km, and (c) 75–80 km for each month.

regarding Sc in the mesosphere, it is assumed in the present analyses that Sc at a given height is constant during PMWE season.

The electron density in the mesosphere strongly depends on SZA. Singer et al. (2011) examined MF radar observations at Andøya (69.30°N, 16.04°E) and showed that the seasonal variation of monthly mean electron density in the height range of 65–80 km at a fixed SZA is small. In addition, occasional increases in electron density associated with irregular or random solar or magnetic disturbances are often observed, resulting in the appearance of PMWE (Kataoka et al., 2019; Nishiyama et al., 2018). We assumed that such short-period variability of electron density associated with random solar or magnetic disturbances would be filtered out by the temporal averages.

In summary, under the two assumptions above, radar volume reflectivity largely depends on ε for an SZA and height with a sufficiently large number of observations. In the following analyses, the focus is on observations for SZAs of 90° to 95° since sufficient data for this SZA range are available in March through October (Figure 7). Note that it was confirmed that the following results do not change significantly for slight changes in the SZA range, such as 95° to 100° or 85° to 90°.

Figure 9 shows the monthly histograms of ε for an SZA interval of 90° to 95° and height ranges of 65–70, 70–75, and 75–80 km. In the height ranges of 65–70 and 70–75 km, the distribution of ε values smaller than 3×10^{-3} m^2 s^{-3} does not change significantly during PMWE season. It is found that the frequency of ε values greater than 3×10^{-2} m^2 s^{-3} is higher in April through August than in March, September, and October. This suggests that the ε has a maximum in winter and becomes smaller in spring and fall, which is consistent with the results from the Arctic rocket observations (Lübken, 1997). It is also interesting that the distributions in April through August are quite similar. This result indicates that the transition of the mesospheric ε from summer to winter occurs in March and that the winter-to-summer transition occurs in September. For the 75–80 km range, the distributions are quite similar in April through July, and the frequency of ε values greater than 3×10^{-2} m^2 s^{-3} in August is relatively small compared to those in April through July. This implies that the winter-to-summer transition of ε in the 75–80 km height range is slightly earlier than in the 65–75 km range.

Yasui et al. (2016) examined the gravity wave activity in the middle and upper mesosphere using an MF radar at Syowa Station and showed that the kinetic energy of the gravity waves is maximized in midwinter. The turbulence in the mesosphere is considered to be mainly caused by gravity wave breaking. The seasonal variation of ε observed in March through October is consistent with this inference. Note that previous studies using MF radars located in the Antarctic region also showed the midwinter maximum of kinetic energy of gravity waves in the mesosphere (e.g., Dowdy et al., 2007; Hibbins et al., 2007). Thus, it is expected that the midwinter maximum of the turbulence intensity should be common in the Antarctic mesosphere.

4. Summary and Concluding Remarks

Using PMWE observations by the PANSY radar at Syowa Station (69.00°S, 39.35°E) recorded over a period of 4 years (2016–2019), we examined the seasonal variation of radar volume reflectivity η and turbulent kinetic energy dissipation rates ε in the mesosphere in March through October. Our analysis provides the first estimates of the turbulence parameters in the Antarctic winter mesosphere. Our results can be summarized as follows:

1. The radar volume reflectivities show a lognormal distribution in the range of 2×10^{-18} to 5×10^{-15} m^{-1} for the height range of 55–82 km. The median value is approximately 3×10^{-17} m^{-1}.

2. The energy dissipation rates derived from the PMWE spectral widths are in the range of 10^{-4} to 10^{0} m^2 s^{-3}. The histogram of ε averaged over the height range of 55–82 km and over the entire analyzed period has a broad peak and does not look lognormal.
3. The height variation of the histograms of ε shows a decrease in the number of ε values smaller than 10^{-2} m^2 s^{-3} above a height of 78 km (Figure 6). This indicates that sufficiently strong turbulence is required for PMWE to be detected by the radar in the high kinematic viscosity conditions at the greater heights.
4. The SZA dependence of the histogram of ε shows that the minimum value of the ε range during the nighttime is significantly greater than that during the daytime (Figure 7). This can be explained by the diurnal variation of electron density. During the nighttime, strong turbulence is required for PMWE to be detected by the radar since electron density is significantly lower at night than during the daytime.
5. From the comparison of monthly histograms of ε for fixed SZA and height, it is found that mesospheric ε is maximized in austral winter and that the summer-to-winter (winter-to-summer) transition of mesospheric ε occurs in March (September) in the 65–75 km height range.

Note that the height and SZA dependence of the distributions of η and ε shown in the present study are qualitatively consistent with the theory that PMWE are attributable to scattering echoes from turbulence in the ionized atmosphere (Hocking, 1983; Lübken et al., 2006, 2007).

Since the turbulence in the mesosphere mainly originates from the breaking of gravity waves, the transition of ε from winter to summer is related to the seasonal variation of the stratospheric polar vortex and final warming. A study of the interannual variability of mesospheric turbulence in terms of the polar vortex would be highly interesting and is planned as a future project.

Data Availability Statement

The PANSY radar observational data are available at the project website (http://pansy.eps.s.u-tokyo.ac.jp/en/archive_data/Kohma_etal_2020, https://doi.org/10.17592/002.2020070384).

Acknowledgments
This study is supported by JSPS KAKENHI Grant JP16K17801/19K14791 and JST CREST Grant JPMJCR1663. PANSY is a multi-institutional project with core members from The University of Tokyo, the National Institute of Polar Research, and Kyoto University. The PANSY radar measurements at Syowa Station are operated by the Japanese Antarctic Research Expedition (JARE). Figure 1 was drawn by software developed by the Dennou-Ruby Davis project. We thank Takuji Nakamura, Takanori Nishiyama, and Ryosuke Yasui for helpful discussions and comments on this work. Finally, we acknowledge three anonymous reviewers for greatly helping us to improve this manuscript.

References

Czechowsky, P., Reid, I. M., Ruster, R., & Schmidt, G. (1989). VHF radar echoes observed in the summer and winter polar mesosphere over Andøya, Norway. *Journal of Geophysical Research*, *94*(D4), 5199–5217. https://doi.org/10.1029/JD094iD04p05199

Dehghan, A., & Hocking, W. K. (2011). Instrumental errors in spectral-width turbulence measurements by radars. *Journal of atmospheric and solar-terrestrial physics*, *73*(9), 1052–1068. https://doi.org/10.1016/j.jastp.2010.11.011

Dowdy, A. J., Vincent, R. A., Tsutsumi, M., Igarashi, K., Murayama, Y., Singer, W., & Murphy, D. J. (2007). Polar mesosphere and lower thermosphere dynamics: Mean wind and gravity wave climatologies. *Journal of Geophysical Research*, *112*, D17104. https://doi.org/10.1029/2006jd008126

Ecklund, W. L., & Balsley, B. B. (1981). Long-term observations of the Arctic mesosphere with the MST radar at Poker Flat, Alaska. *Journal of Geophysical Research*, *86*(A9), 7775–7780. https://doi.org/10.1029/JA086iA09p07775

Fukao, S., Hamazu, K., & Doviak, R. J. (2014). *Radar for meteorological and atmospheric observations*. Tokyo: Springer.

Gregg, M. C., D'Asaro, E. A., Riley, J. J., & Kunze, E. (2018). Mixing efficiency in the ocean. *Annual Review of Marine Science*, *10*, 443–473. https://doi.org/10.1146/annurev-marine-121916-063643

Hall, C. M., Hoppe, U. P., Blix, T. A., Thrane, E. V., Manson, A. H., & Meek, C. E. (1999). Seasonal variation of turbulent energy dissipation rates in the polar mesosphere: A comparison of methods. *Earth, Planets and Space*, *51*(7–8), 515–524. https://doi.org/10.1186/Bf03353212

Hibbins, R. E., Espy, P. J., & Jarvis, M. J. (2007). Quasi-biennial modulation of the semidiurnal tide in the upper mesosphere above Halley, Antarctica. *Geophysical Research Letters*, *34*, L21804. https://doi.org/10.1029/2007gl031282

Hocking, W. K. (1983). On the extraction of atmospheric-turbulence parameters from radar backscatter Doppler spectra—I. Theory. *Journal of Atmospheric and Terrestrial Physics*, *45*(2-3), 89–102. https://doi.org/10.1016/S0021-9169(83)80013-0

Hocking, W. K. (1985). Measurement of turbulent energy dissipation rates in the middle atmosphere by radar techniques: A review. *Radio Science*, *20*(6), 1403–1422. https://doi.org/10.1029/RS020i006p01403

Hocking, W. K. (1999). The dynamical parameters of turbulence theory as they apply to middle atmosphere studies. *Earth, Planets and Space*, *51*(7–8), 525–541. https://doi.org/10.1186/Bf03353213

Hocking, W. K., Röttger, J., Palmer, R. D., Sato, T., & Chilson, P. B. (2016). *Atmospheric radar: Application and science of MST radars in the Earth's mesosphere, stratosphere, troposphere, and weakly ionized regions*. Cambridge: Cambridge University Press.

Holdsworth, D. A., Vincent, R. A., & Reid, I. M. (2001). Mesospheric turbulent velocity estimation using the Buckland Park MF radar. *Annales de Geophysique*, *19*(8), 1007–1017. https://doi.org/10.5194/angeo-19-1007-2001

Kantha, L., & Luce, H. (2018). Mixing coefficient in stably stratified flows. *Journal of Physical Oceanography*, *48*(11), 2649–2665. https://doi.org/10.1175/Jpo-D-18-0139.1

Kataoka, R., Nishiyama, T., Tanaka, Y., Kadokura, A., Uchida, H. A., Ebihara, Y., et al. (2019). Transient ionization of the mesosphere during auroral breakup: Arase satellite and ground-based conjugate observations at Syowa Station. *Earth, Planets and Space*, *71*(1), 1–10. https://doi.org/10.1186/s40623-019-0989-7

Kavanagh, A. J., Honary, F., Rietveld, M. T., & Senior, A. (2006). First observations of the artificial modulation of polar mesospheric winter echoes. *Geophysical Research Letters*, *33*, L19801. https://doi.org/10.1029/2006gl027565

Kirkwood, S. (2007). Polar mesosphere winter echoes—A review of recent results. *Advances in Space Research*, *40*(6), 751–757. https://doi.org/10.1016/j.asr.2007.01.024

Kirkwood, S., Belova, E., Blum, U., Croskey, C., Dalin, P., Fricke, K. H., et al. (2006). Polar mesosphere winter echoes during MaCWAVE. *Annales de Geophysique*, *24*(4), 1245–1255. https://doi.org/10.5194/angeo-24-1245-2006

Kirkwood, S., Chilson, P., Belova, E., Dalin, P., Häggström, I., Rietveld, M., & Singer, W. (2006). Infrasound—The cause of strong polar mesosphere winter echoes? *Annales de Geophysique*, *24*(2), 475–491. https://doi.org/10.5194/angeo-24-475-2006

La Hoz, C., & Havnes, O. (2008). Artificial modification of polar mesospheric winter echoes with an RF heater: Do charged dust particles play an active role? *Journal of Geophysical Research*, *113*, D19205. https://doi.org/10.1029/2008jd010460

Latteck, R., Renkwitz, T., & Strelnikov, B. (2019). D region observations by VHF and HF radars during a rocket campaign at Andøya dedicated to investigations of PMWE. *Advances in Radio Science*, *17*, 225–237. https://doi.org/10.5194/ars-17-225-2019

Latteck, R., & Strelnikova, I. (2015). Extended observations of polar mesosphere winter echoes over Andøya (69°N) using MAARSY. *Journal of Geophysical Research: Atmospheres*, *120*, 8216–8226. https://doi.org/10.1002/2015jd023291

Lübken, F. J. (1997). Seasonal variation of turbulent energy dissipation rates at high latitudes as determined by in situ measurements of neutral density fluctuations. *Journal of Geophysical Research*, *102*(D12), 13,441–13,456. https://doi.org/10.1029/97JD00853

Lübken, F. J. (2014). Turbulent scattering for radars: A summary. *Journal of Atmospheric and Terrestrial Physics*, *107*, 1–7. https://doi.org/10.1016/j.jastp.2013.10.015

Lübken, F. J., Singer, W., Latteck, R., & Strelnikova, I. (2007). Radar measurements of turbulence, electron densities, and absolute reflectivities during polar mesosphere winter echoes (PMWE). *Advances in Space Research*, *40*(6), 758–764. https://doi.org/10.1016/j.asr.2007.01.015

Lübken, F. J., Strelnikov, B., Rapp, M., Singer, W., Latteck, R., Brattli, A., et al. (2006). The thermal and dynamical state of the atmosphere during polar mesosphere winter echoes. *Atmospheric Chemistry and Physics*, *6*, 13–24. https://doi.org/10.5194/acp-6-13-2006

Morris, R. J., Klekociuk, A. R., & Holdsworth, D. A. (2011). First observations of Southern Hemisphere polar mesosphere winter echoes including conjugate occurrences at ~69°S latitude. *Geophysical Research Letters*, *38*, L03811. https://doi.org/10.1029/2010gl046298

Nastrom, G. D. (1997). Doppler radar spectral width broadening due to beamwidth and wind shear. *Annales de Geophysique*, *15*(6), 786–796. https://doi.org/10.1007/s005850050497

Nastrom, G. D., & Eaton, F. D. (1997). Turbulence eddy dissipation rates from radar observations at 5–20 km at White Sands Missile Range, New Mexico. *Journal of Geophysical Research*, *102*(D16), 19,495–19,505. https://doi.org/10.1029/97jd01262

Nishimura, K., Kohma, M., Sato, K., & Sato, T. (2020). Spectral observation theory and beam debroadening algorithm for atmospheric radar. *IEEE Transactions on Geoscience and Remote Sensing*. https://doi.org/10.1109/TGRS.2020.2970200

Nishiyama, T., Sato, K., Nakamura, T., Tsutsumi, M., Sato, T., Kohma, M., et al. (2015). Height and time characteristics of seasonal and diurnal variations in PMWE based on 1 year observations by the PANSY radar (69.0°S, 39.6°E). *Geophysical Research Letters*, *42*, 2100–2108. https://doi.org/10.1002/2015gl063349

Nishiyama, T., Sato, K., Nakamura, T., Tsutsumi, M., Sato, T., Tanaka, Y. M., et al. (2018). Simultaneous observations of polar mesosphere winter echoes and cosmic noise absorptions in a common volume by the PANSY radar (69.0°S, 39.6°E). *Journal of Geophysical Research: Atmospheres*, *123*, 5019–5032. https://doi.org/10.1029/2017ja024717

Picone, J. M., Hedin, A. E., Drob, D. P., & Aikin, A. C. (2002). NRLMSISE-00 empirical model of the atmosphere: Statistical comparisons and scientific issues. *Journal of Geophysical Research*, *107*(A12), 1468. https://doi.org/10.1029/2002ja009430

Rapp, M., Gumbel, J., Lübken, F. J., & Latteck, R. (2002). *D* region electron number density limits for the existence of polar mesosphere summer echoes. *Journal of Geophysical Research*, *107*(D14), 4187. https://doi.org/10.1029/2001jd001323

Sato, K., Hashiguchi, H., & Fukao, S. (1995). Gravity waves and turbulence associated with cumulus convection observed with the UHF/VHF clear-air Doppler radars. *Journal of Geophysical Research*, *100*(D4), 7111–7119. https://doi.org/10.1029/95jd00198

Sato, K., Kohma, M., Tsutsumi, M., & Sato, T. (2017). Frequency spectra and vertical profiles of wind fluctuations in the summer Antarctic mesosphere revealed by MST radar observations. *Journal of Geophysical Research: Atmospheres*, *122*, 3–19. https://doi.org/10.1002/2016jd025834

Sato, K., Tomikawa, Y., Nishimura, K., & Sato, T. (2019). Estimate of turbulent energy dissipation rate from the VHF radar and radiosonde observations in the Antarctic. *Journal of Geophysical Research*, *124*, 2976–2993. https://doi.org/10.1029/2018jd029521

Sato, K., Tsutsumi, M., Sato, T., Nakamura, T., Saito, A., Tomikawa, Y., et al. (2014). Program of the Antarctic Syowa MST/IS radar (PANSY). *Journal of Atmospheric and Solar-Terrestrial Physics*, *118*, 2–15. https://doi.org/10.1016/j.jastp.2013.08.022

Sato, T., & Woodman, R. F. (1982). Fine altitude resolution observations of stratospheric turbulent layers by the Arecibo 430 MHz radar. *Journal of the Atmospheric Sciences*, *39*(11), 2546–2552. https://doi.org/10.1175/1520-0469(1982)039<2546:FAROOS>2.0.CO;2

Singer, W., Latteck, R., Friedrich, M., Wakabayashi, M., & Rapp, M. (2011). Seasonal and solar activity variability of *D*-region electron density at 69°N. *Journal of Atmospheric and Solar-Terrestrial Physics*, *73*(9), 925–935. https://doi.org/10.1016/j.jastp.2010.09.012

Strelnikova, I., & Rapp, M. (2013). Statistical characteristics of PMWE observations by the EISCAT VHF radar. *Annales de Geophysique*, *31*(2), 359–375. https://doi.org/10.5194/angeo-31-359-2013

Tsutsumi, M., Sato, K., Sato, T., Kohma, M., Nakamura, T., Nishimura, K., & Tomikawa, Y. (2017). Characteristics of mesosphere echoes over Antarctica obtained using PANSY and MF radars. *Sola*, *13a*, 19–23. https://doi.org/10.2151/sola.13A-004

Weinstock, J. (1981). Using radar to estimate dissipation rates in thin-layers of turbulence. *Radio Science*, *16*(6), 1401–1406. https://doi.org/10.1029/RS016i006p01401

Yasui, R., Sato, K., & Tsutsumi, M. (2016). Seasonal and interannual variation of mesospheric gravity waves based on MF radar observations over 15 years at Syowa Station in the Antarctic. *Solaiat*, *12*, 46–50. https://doi.org/10.2151/sola.2016-010